Chlorinated phosphorene for energy application

Chlorinated phosphorene for energy application: electronic and phonon properties

N. Hassani,[1,*] M. Yagmurcukardes,[2] F. M. Peeters,[3,4] and M. Neek-Amal[1,5,†]

[1] *Department of Physics, Shahid Rajaee Teacher Training University, 16875-163 Lavizan, Tehran, Iran.*
[2] *Department of Photonics, Izmir Institute of Technology, 35430 Izmir, Turkey.*
[3] *Departamento de Física, Universidade Federal do Ceará, 60455-760 Fortaleza, Ceará, Brazil.*
[4] *HSE University, Moscow, 101000 Russia.*
[5] *Departement Fysica, Universiteit Antwerpen, Groenenborgerlaan 171, B-2020 Antwerpen, Belgium.*

(Dated: October 3, 2022)

The influence of doping impurities and the composition-dependent band gap in 2D materials has been the subject of debate for a long time. Here, by using Density Functional Theory (DFT) calculations, we systematically disclose physical propertiese chlorinated phosphorene having the stoichiometry of P_mCl_n. By analyzing the contribution from the adsorption energy, charge density differences, migration energy barrier, structural, vibrational, and electronic properties of the chlorinated phosphorene, we found that (1) the $Cl-P$ bonds are strong with binding energy E_b =-1.61 eV, (2) Cl atoms on phosphorene have anionic feature, (3) the migration path of Cl on phosphorene is anisotropic with an energy barrier of 0.38 eV, (4) the phonon band dispersion reveal that the chlorinated phosphorenes are stable when $r \leq 0.25$ where $r = m/n$, (5) the chlorinated phosphorenes may be used as a photonic crystal in the frequency range of 280 cm^{-1} to 325 cm^{-1}, (6) the electronic band structure of the all chlorinated phosphorenes has some flat bands emerging around the Fermi level with widths in the range of 22 meV to 580 meV, and (7) Cl adsorption causes the semiconducting to the metallic/semi-metallic transition which increases the electrical conductivity, suitable for application as an electroactive material. To examine this application, we investigated the change in binding energy, specific capacity, and open-circuit voltage as a function of the density of adsorbed Cl. It is found that E_b decreases with increasing Cl content. The theoretical storage capacity of the chlorinated phosphorene is calculated to be 168.19 mA h g^{-1} with a large average voltage of 2.08 V which is ideal to be used as a cathode in the chloride-ion batteries. These results indicate that phosphorene is a promising 2D-material for application in the electronic and phononic devices.

I. INTRODUCTION

Phosphorene sheets are the constituent layers of black phosphorus that stack with van der Waals (vdW) interactions. The crystal type of phosphorene is orthorhombic and the atoms are connected to each other in a chair-like structure [1–3]. Among 2D-materials, black phosphorus and especially its halogenated counterparts have broad application prospects [4–7]. For example, it was shown that the halogenated phosphorene bilayer can be applied as the long-sought 2D-multiferroic metal-free system. In such system, vertical polarization can be controlled against depolarizing field, which is needed for data storage [8].

Also, phosphorene halides were theoretically revealed to have significant oxidation resistance and desirable electronic and optical properties. For instance, α-P_3Cl_2 is shown to be a direct semiconductor with a band gap of 2.41 eV and has a highly anisotropic carrier mobility (56,890 $\mathrm{cm}^2\,\mathrm{V}^{-1}\,\mathrm{s}^{-1}$ for electron and 26,450 $\mathrm{cm}^2\,\mathrm{V}^{-1}\,\mathrm{s}^{-1}$ for hole) witch enable it for visible-light water splitting [9]. Moreover, phosphorene was repeatedly proposed as an electroactive material in various rechargeable batteries [10–12]. In a theoretical work, Pu *et al.* [13] investigated that Cl (F, Br) and I doped phosphorenes are p-type/direct and n-type/indirect semiconductors. Also, they investigated that Cl- and I-phosphorenes are promising spin-gapless semiconductors. It was revealed that the halogen-striped functionalized monolayer has a wedge energy band when the stripe–stripe distance was less than 40 Å . The latter leads to the linear relation between energy and momentum that can be used in optics-like nano-electronics [14].

It was also reported that graphene can be fully chlorinated, resulting in a stable structure called chlorographene. In this structure, each hexagon has six chlorine atoms that are alternatingly bonded at top and bottom of the graphene surface with sp^3-type covalent bonds [15]. However, there is a lack of knowledge about the effect of gradually increasing Cl concentration on phosphorene and corresponding electronic properties. From the application point of view, although extensively literature have been published on the application of black phosphorus and phosphorene in rechargeable batteries, phosphorene has not been experimentally and theoretically evaluated as an electroactive material in chloride ion batteries (ClBs).

In this work, we theoretically study the electronic structure of chlorinated phosphorene and predict that it can be a cathode material in ClBs. The cathode performance is examined by changing the content of Cl adsorbed on phosphorene. In order to investigate the properties of chlorinated phosphorene, the optimized structure, adsorption energy, electronic band structure, elec-

* nasim.hassani.chem@gmail.com
† mehdi.neekamal@gmail.com

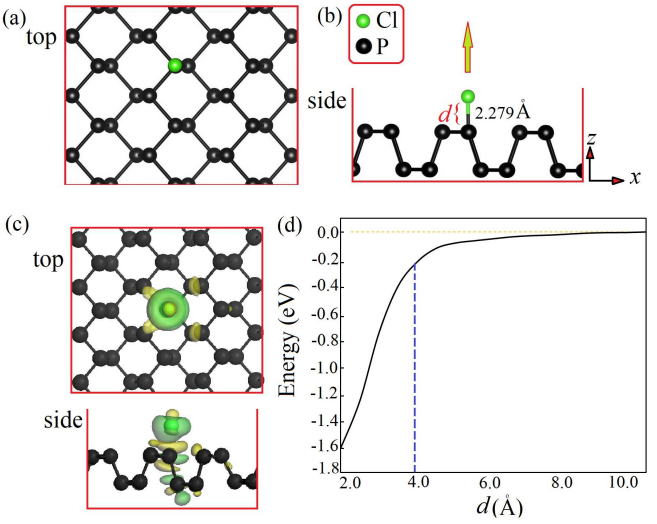

Figure 1. (a) Top and side (b) views of the most stable binding site of Cl atom on a 3 × 3 supercell of phosphorene. (c) Top and side views of the charge density difference between Cl and phosphorene with the isovalue of 0.02 $|e|/\text{Å}^3$. Yellow and green colors show charge deficient and charge sufficient, respectively. (d) The change of total energy of Cl on phosphorene surface with respect to Cl–phosphorene distance (d) along z-axis as schematically shown in panel (b).

tronic density of states, charge transfer, phonon band structure, and phonon density of states are calculated .

II. THE METHOD

All calculations were carried out using CASTEP package as implemented in the Material Studio software [16]. The density functional theory (DFT) framework with the generalized gradient approximation (GGA) and Perdew–Burke–Ernzerhof (PBE) functional were used to consider the electron exchange-correlation interactions [17]. Long-range vdW interactions were considered by using Grimme's empirical dispersion corrected method [18]. The valence electron configurations for P and Cl were chosen to be $3s^2 3p^3$ and $3s^2 3p^5$, respectively. The cut-off energy of 600 eV was considered for the plane-wave basis. the stress-free configurations were obtained through full optimization, i.e, atomic positions and lattice vectors using a conjugate gradient algorithm.

The change in energy and force throughout the relaxation was considered to be 0.01 meV and 0.01 eV Å^{-1}, respectively. A vacuum space of 20 Å was inserted along the z-axis to eliminate specular interactions from adjacent layers. The orbital calculation of $DMol^3$ package was also used to compute the difference in charge density between Cl atom and phosphorene [19].

The binding energy per Cl-atom (E_b), for a system with a unit cell containing m number of P and n number of Cl, can be calculated as follows:

$$E_b = (E_{Total} - E_{P_m} - n\,E_{Cl})/n, \tag{1}$$

where E_{Total}, E_{P_m}, and E_{Cl} refer to the energy of Cl/phosphorene complex, the bare phosphorene with m number of phosphorus atoms, and a Cl atom, respectively. Notice that in this study $m_{max} = 36$ and $n_{max} = 2$, i.e., we simply decrease the density of Cl by making the simulation cell larger. When $E_b < 0$ an energetically favorable interaction between Cl and phosphorene is emerged leading to a stable structure.

The Arrhenius equation was used to study the molecular transition rate (R) that can be evaluated using the following expression:

$$R \sim e^{-E_a/k_B T}, \tag{2}$$

where T, E_a, and k_B indicate temperature, the diffusion energy barrier, and Boltzmann's constant, respectively.

Open-circuit-voltage (V_{OCV}) is widely used to determine the performance of batteries. The V_{OCV} curve can be obtained by calculating the average voltage over the Cl content. The average voltage (V) of the system $P_m Cl_n$ ($r = m/n$) in the range of $r_1 \le r \le r_2$ was approximated by

$$V \approx \frac{E(Cl_{r_1}P) - E(Cl_{r_2}P) + (r_2 - r_1)E(Cl)}{e(r_2 - r_1)}. \tag{3}$$

It is important to mention that V_{OCV} can be calculated from the Gibbs free energy; however, if the change of volume and entropy is negligible, one can calculate V_{OCV} from the energy differences (Eq. (3)) [20].

III. RESULTS AND DISCUSSION

A. Adsorption of Cl on phosphorene

We performed geometry optimizations considering adsorption on different sites of phosphorene surface to explore energetically more favorable sites for Cl adsorption. The results of optimized lattice constants (a, b) for different content of Cl on phosphorene are given in Table I. As shown in Fig. 1(a, b), the most stable adsorption site for Cl on a 3×3 supercell of phosphorene, is directly above the P atom of an uppermost atomic layer at a distance of $d = 2.279$ Å in good agreement with literature [4].

The calculated E_b value for Cl/phosphorene complex is found to be about -1.61 eV. This negative value refers to the exothermic reaction between the Cl atom and phosphorene. The formation energy of Cl_2 is 1.26 eV per molecule [15], indicating that the Cl atom would be adsorbed on phosphorene surface rather than forming Cl dimer or Cl-clusters. This binding energy is even larger than the adsorption of Cl on a graphene surface (1.16 eV) [15].

The spatial charge density difference between Cl and phosphorene is shown in Fig. 1(c). The large sufficiency

Table I. The calculated lattice constants for phosphorene and its Cl doped counterparts, a and b (in Å); the electronic band gap, Δ (in eV); the phonon band gap, δ (in cm^{-1}); the flat band (FB) width, W_{FB} (in meV); the spin splitting of FB, SS_{FB} (in eV) the average charge on Cl atom ; q_{Cl}, average $P-Cl$ bond length (in Å), theoretical specific capacity; Q (in mA h g^{-1}); estimated open-circuit voltage, V_{OCV} (in V).

systems↓ properties→	a	b	Δ	δ	W_{FB}	SS_{FB}	q_{Cl}	$P-Cl$	Q	V_{OCV}
phosphorene	3.281	4.857	1.11	45.73	-	-	-	-	-	-
r=0.042	10.147	13.195	0.00	40.53	281	0.22	-0.20	2.279	34.41	2.39
(1)* r=0.055	10.147	13.195	0.25	12.01	103	0.25	-0.19	2.295	45.20	2.39
(2) r=0.055	10.147	13.195	0.76	19.18	176	0.07	-0.10	2.137	45.20	2.39
r=0.083	6.591	9.484	0.00	24.15	260	0.13	-0.14	2.210	65.83	2.34
(1) r=0.125	6.582	9.733	0.99	40.20	50	0.30	-0.09	2.132	121.11	2.28
(2) r=0.125	6.596	9.421	0.44	80.62	22	0.45	-0.10	2.154	121.11	2.28
(3) r=0.125	6.609	9.490	1.26	56.16	92	0.14	-0.10	2.121	121.11	2.28
r=0.187	6.603	9.478	0.00	68.52	297	0.43	-0.09	2.133	133.57	1.85
(1) r=0.25	3.382	4.398	0.00	65.97	305	0.56	-0.09	2.154	168.19	1.56
(2) r=0.25	4.398	6.765	0.93	65.24	580	0.44	-0.08	2.119	168.19	1.56
(3) r=0.25	4.398	6.765	0.25	78.58	404	0.43	-0.07	2.125	168.19	1.56
(4) r=0.25	4.398	6.765	0.71	90.71	262	0.29	-0.10	2.164	168.19	1.56
$BiCl_3$ [21]									176.5	2.4
$Co_3^{2+}Fe^{3+}(OH)_8Cl{\cdot}1.6H_2O$ [22]									62.0	-
$Co_3^{2+}Fe^{3+}(OH)_8Cl_4{\cdot}1.6H_2O$ [22]									198.7	-
PPyCl@CNTs [23]									115.0	2.2
BiOCl [24]									103.1	2.2
FeOCl [25]									250.0	2.2

*The numbers in parentheses in the first column refer to the different structures for the same value of r (see Fig. 3, Figs. S1 and S2)

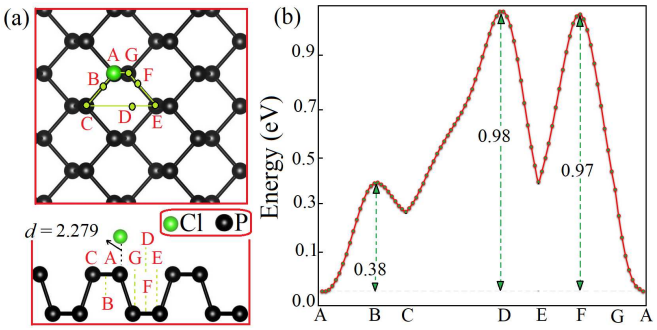

Figure 2. (a) Schematic top and side views of Cl migration path. The corresponding positions are named by alphabets. (b) Energy profile of Cl migration on phosphorene surface. The corresponding energy barriers are shown in the figure.

of charge around the Cl atom indicates charge transfer from phosphorene to the Cl atom. Charge donation occurs only between the Cl and six P atoms that are chemically bonded to each other and are close to the Cl atom. Hirshfeld charge analysis shows that for Cl on 3×3 supercell of phosphorene, P atoms possess about $0.20\,|e|$ from their $3p$ orbital to the $3p$ orbital of the Cl atom. Therefore, the Cl atom on phosphorene surface is an anion. However, as the content of the Cl atom on one or both sides of the phosphorene increases, the charge transferred from the P atoms to the Cl atom decreases to $0.07\,|e|$ (see Table 1).

Next, we move Cl atom far from its most stable binding to about 12.79 Å perpendicular to the phosphorene surface to show the distance dependence of E_b (see Fig. 1(d)). For the distances beyond 6 Å, the binding energy is negligible. In contrast, at distances less than 4 Å, the interaction between Cl and phosphorene sheet is attractive where the energy decreases with a steep slope which is shown by dashed blue line in Fig. 1(d). Thus, it is obvious that Cl adsorption on phosphorene is a barrierless process.

B. Migration of Cl on phosphorene

The mobility of Cl on phosphorene plays an important role in the stability and arrangement of Cl on its surface. Therefore, we studied Cl migration on the phosphorene surface. A 3×3 supercell of phosphorene is used to study Cl migration on it, where $r = 0.042$. The minimum energy path of Cl diffusion on phosphorene is obtained where at each point on the energy curve, x- and y-positions of the Cl atom are considered to be fixed and relaxation is allowed along z-direction by minimizing the total energy and atomic forces.

From the top view of phosphorene, the atoms are arranged in a honeycomb lattice in which the anisotropy of the structure directs the migration of Cl on its surface. As mentioned above, Cl adsorbs on top of a P atom. Hence, the symmetry of the structure, we considered a path starting from A and ending to A as illustrated in Fig. 2(a), in order to predict Cl migration on phosphorene. The corresponding plot of the energy change along the migration path is shown in Fig. 2(b). The Cl atom can diffuse onto adjacent Cl atoms (A to C) by passing over an energy barrier (E_a) of 0.38 eV (at position B).

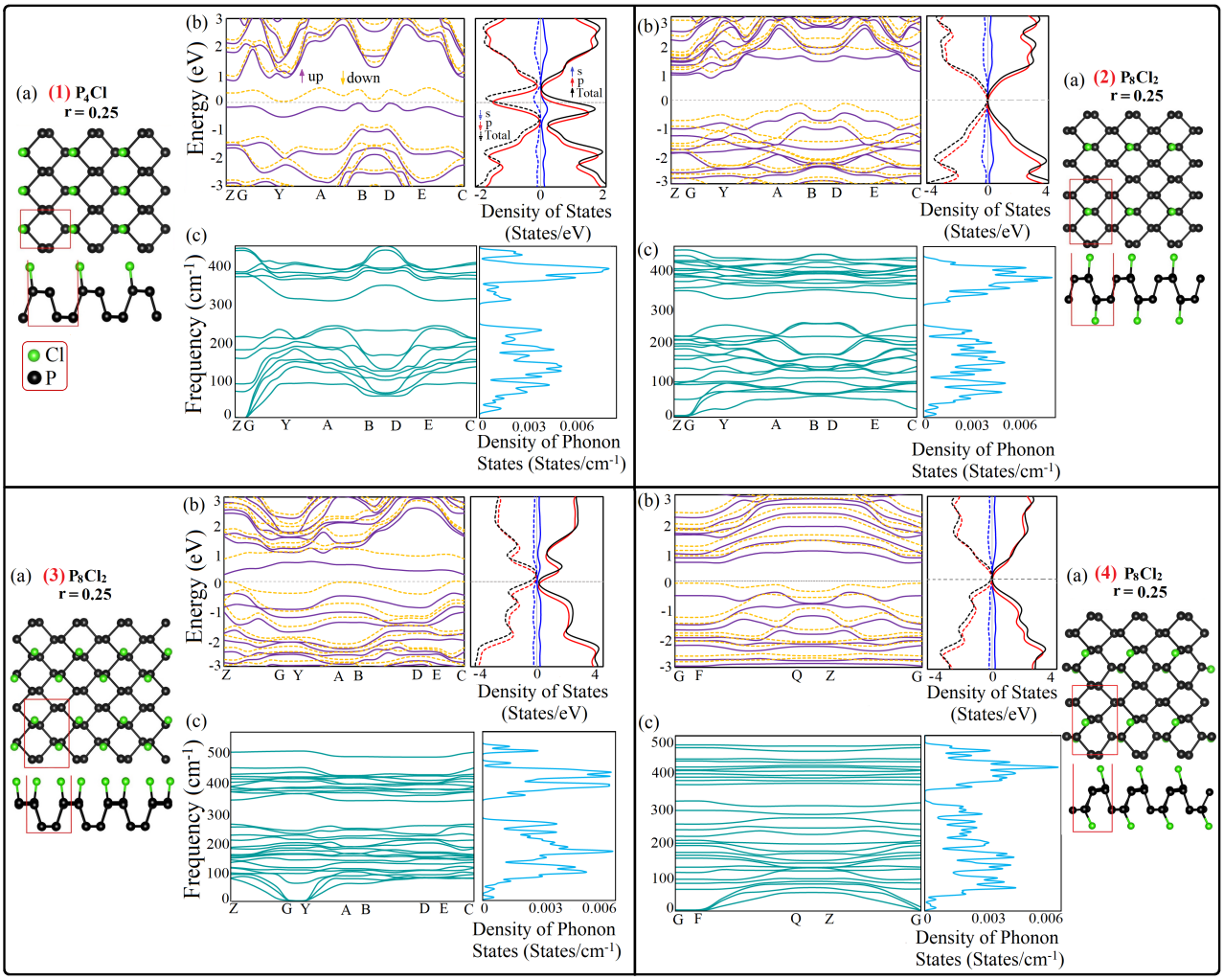

Figure 3. Top and side views of P_mCl_n ($r = m/n = 0.25$) with Cl bonded on one or two sides are shown in the corner of each panel. The electronic band structure (Left) and the electronic density of states (Right) are depicted in the top of each panel. The phonon band structure (Left) and the phonon density of states (Right) are demonstrated in the bottom of each panel. The numbers in parentheses refer to the different structures for the r value of 0.25 (see Table I).

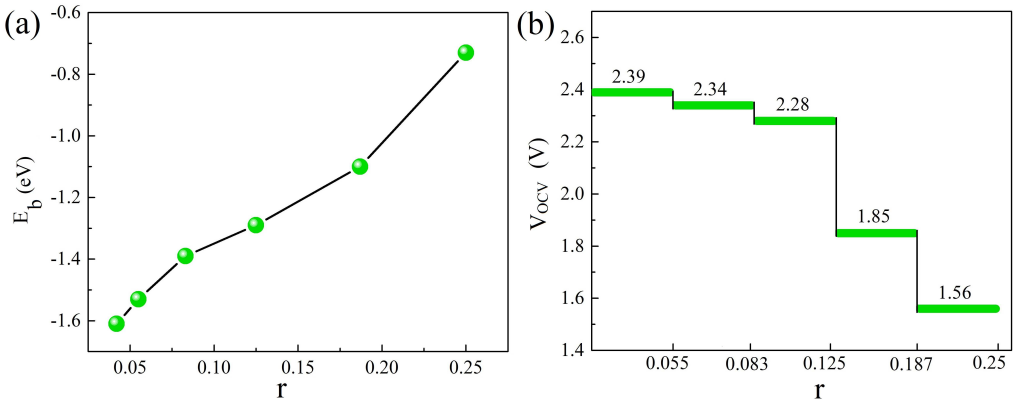

Figure 4. (a) Binding energies per Cl-atom (E_b) as a function of Cl content. (b) Open-circuit voltage (V_{OCV}) profile with respect to Cl content from 0 to 0.25. Notice that here E_b is the total binding energy per Cl-atom of the unit cell with m number of P and n number of Cl.

Then Cl can migrate along the diagonal of the honeycomb (C to E) with the E_a of 0.98 eV relative to the first position (A). Finally, Cl can diffuse on phosphorene from E to A by overcoming an $E_a = 0.97$ eV.

Our results show that the most likely diffusion path of Cl on phosphorene is between two adjacent P atoms due to the lower energy barrier. However, the migration of Cl on phosphorene has a strong directional anisotropy feature because of the puckered phosphorene structure. Using Eq. (2), the transition rate of Cl from A to C is about 9.40×10^9 faster than that of other paths at room temperature. This indicates an extremely low probability of Cl migration anywhere except between two adjacent P atoms.

C. Electronic and phononic properties of chlorinated phosphorene

To examine the effect of Cl concentration on the electronic properties of phosphorene, we considered different stable structures having the stoichiometry of P_mCl_n ($r = n/m$ = 0.042, 0.055, 0.083, 0.125, 0.187, 0.25) as shown in Fig. 3(a), and Figs. S1 and S2(a) of supporting information (SI) file. For the different values of r, we have considered supercells with different sizes: r=0.042: one Cl atom bonded on one side of a 3×3 supercell, r=0.055: two Cl atoms bonded on one or two sides of a 3×3 supercell (two structures), r=0.083: one Cl atom bonded on one side of a 2×2 supercell, r=0.125: two Cl atoms bonded on one or two sides of a 2×2 supercell (three structures), r=0.187: three Cl atoms bonded on both sides of a 2×2 supercell, r=0.25: one Cl atom bonded on one side of a 1×1 supercell or two Cl atoms bonded on one or two sides of a 1×2 supercell (four structures).

We have evaluated the electronic properties of Cl-doped phosphorene with different values of r by means of band structure analysis. Figure. 3(b), Figs. S1-S3(b) illustrate the calculated electronic band structure and partial density of states (PDOS) for pristine phosphorene and the structures with the different r values. Our results indicate that pristine phosphorene is a semiconductor with a band gap (Δ) of 1.11 eV (see Fig. S3) in good agreement with the other theoretical works [26, 27]. However, Cl-doping on phosphorene surface can drastically alter the electronic feature of pristine phosphorene. For odd numbers of Cl, the structure shows metallic behaviour and for even numbers of Cl atoms, Δ ranges from 0.25 to 1.26 eV. Phosphorene was also found to exhibit semiconductor to metal transition for metal ion intercalation [28]. For all chlorinated phosphorene, the p orbitals are dominant and has a strong contribution near the Fermi level.

As listed in Table I, there are four structures for r = 0.25. Our results indicate that all these structures have metallic or semi-metallic behaviour. This infers that the metallic behavior of phosphorene increase monotonically with increasing Cl doping up to the ratio of 0.25. Also, the Δ of phosphorene can be tuned upon Cl doping.

Interestingly, it is found that for all chlorinated phosphorene a nearly flat band (FB) emerges around the Fermi level. In fact, as the PDOS profiles illustrate, the p orbitals dominate the states around the Fermi level, accordingly, the FBs mainly originats from the electrons in the p orbitals. The majority of Cl-doped phosphorene are in the ferromagnetic states due to the asymmetry profile of PDOS. Also, the width of FBs (W_{FB}) for the chlorinated phosphorene is in the range of 22 meV to 580 meV (see Table I). The structures with r=0.125 have narrower FBs. The spin splitting (SS_{FB}) of the FB is in the range of 0.07 to 0.56 eV (see Table I).

The phonon density of states and phonon band structures of pristine phosphorene and its chlorinated counterparts are shown in Fig. 3(c), and Figs. S1-S3(c). All the phonon branches have real eigenfrequencies and therefore all the studied structures (r_{max}=0.25) are expected to be stable. The frequencies are in the range of 15 cm^{-1} to 500 cm^{-1}. Also, the highest frequency of phosphorene does not change drastically as compared to that of chlorinated phosphorene. Generally, photonic crystals are used to allow or prohibit the propagation of electromagnetic waves in certain frequency ranges [29, 30]. The phonon band gap (δ) of chlorinated structures is in the range of 12.01 cm^{-1} to 90.71 cm^{-1}. However, most of these gaps lie between frequencies in the range of 280 cm^{-1} to 325 cm^{-1}, indicating that chlorinated phosphorene could be used as a photonic crystal to influence electromagnetic wave propagation in this frequency range.

We found that the structures of Cl bonded to phosphorene for $r > 0.25$ are unstable. This instability may raise from the remarkable electrostatic repulsive interactions between adjacent Cl anions. Therefore, the insertion of higher contents of Cl into phosphorene leads to cleavage of the $P - P$ bond, which is an irreversible process and decreases chlorination/dechlorination in phosphorene.

D. Possible application of chlorinated phosphorine as cathode in chloride ion battery

Rechargeable batteries are increasing in importance in order to meet the ever-increasing demand for renewable energy caused by the reduced supply of fossil fuels. During the last decades, metal-ion (e.g. Li^+, Na^+, and K^+) rechargeable batteries have attracted much attention due to their outstanding properties such as long cycle life, high energy density, long durability, excellent safety, and no memory effect [31–33]. In contrast, research on anion-based rechargeable batteries has rarely been reported. In this sense, rechargeable batteries based on the shuttling of fluorine and chlorine anions have several key advantages to meet the increasing energy storage requirements [34].

These fascinating features arise from the high electronegativity and appropriate ion radius of these anions. The latter lead to an easier mass transfer, a large the-

oretical volumetric energy density (up to 2500 Wh L^{-1}), a dendrite-free structure, and a wide window of electrochemical stability [35, 36]. In addition, rechargeable batteries based on shuttling of Cl^- (ClBs) have low-cost , large-scale energy storage capacity, and can be manufactured because of the abundance of chloride.

In the pioneering work on ClBs [21], the cathode and anode were chosen to be a metal chloride salt ($BiCl_3$, VCl_3, $CuCl_2$, and $CoCl_2$) and metallic lithium (or magnesium), respectively. Subsequently, metal oxychlorides [37–40], such as $BiOCl$, $VOCl$, $FeOCl$, and $Sb_4O_5Cl_2$, layered double hydroxides [22, 35, 41, 42], antimony-decorated reduced graphene oxide [43], and chloride-doped organic polymers [23, 44], such as polypyrrole (PPy) and polyaniline (PANI), which have been introduced as electroactive materials in ClBs. The reactions that occur during a discharge process at the cathode and anode of a ClB can be expressed as follows [37]:

$$\text{Cathode: } MCl_n + n\,e^- \leftrightarrow M + n\,Cl^-$$
$$\text{Anode: } M' + n\,Cl^- \leftrightarrow M'\,Cl_l + n\,e^-$$

where MCl_n refers to an electroactive cathode material and M' refers to a highly electropositive metal at the anode.

Despite progress in ClBs, cathode materials still have serious problems, including dissolution in the electrolytes, short cyclic life, unsatisfactory electrochemical performance, low capacity, poor structural stability, and large volume expansion. Therefore, the exploration of suitable host cathode material containing high capacity and cycle life to improve ClBs is a top priority. In the following section, we evaluate phosphorene as a possible cathode in ClBs.

1. *Theoretical capacity and voltage profile of chloride in phosphorene*

We found that Cl loading on phosphorene surface is a barrier-less process that makes phosphorene a good candidate for ClBs. Also, a strong E_b is required in the interaction between the electroactive materials and the shuttling atoms. To explore the potential of phosphorene as a cathode in ClBs, we calculated E_b as a function of Cl content and show the results in Fig. 4(a). It is seen that E_b decreases almost linearly with increasing r. For all r values, E_b is larger than 0.71 eV. However, the absolute values of E_b decrease with increasing Cl content, suggesting that the Cl/phosphorene complex becomes less stable due to increasing repulsive interactions between adjacent Cl anions. This trend was also observed for Li-ion, and Mg-ion batteries adsorbed on phosphorene [45, 46]. Depending on the size and induced charge to the cation/anion this trend can be different. Also, the absolute value of E_b for anions is larger than that of cations [28, 45, 47].

As mentioned above, r=0.25 is the high stoichiometry value for Cl/phosphorine complex. Our results indicate that it is equal to a specific capacity of 168.19 mA h g^{-1}. This capacity is comparable to the other cathode materials that have been used in ClBs (see bottom panel of Table 1).

For a series of r values, the average insertion potential V_{OCV} and charging voltage profiles can be estimated. The results of V_{OCV} are shown in Fig. 4(b). The V_{OCV} for Cl-doped phosphorene is explored by considering the following half-cell reaction:

$$PCl_n + n\,e^- \leftrightarrow P + n\,Cl^-. \tag{4}$$

The V_{OCV} decays with a sharp slope from 2.28 V to 1.85 V when $r > 0.125$, and then the slope of the voltage profile becomes slow. The average storage voltage of Cl in phosphorene is found to be 2.08 V. This is promising for phosphorene to be applied as a cathode in ClBs (see Table I).

IV. CONCLUDING REMARKS

To summarize, we performed DFT calculations to study the influence of gradually increasing Cl content on the electronic and phononic properties of phosphorene, i.e. partially chlorinated phosphorene (P_mCl_n). These systems were proposed to have application as a cathode in chloride-ion based batteries (ClBs). Our results show that the Cl atom can be strongly adsorbed on phosphorene with a binding energy of -1.61 eV. Due to the puckered structure of phosphorene, Cl migration shows a highly anisotropic feature with an energy barrier of $E_a = 0.38$ eV. The analysis of electronic band structure, phonon band structure, and density of states revealed that the chlorinated phosphorene are stable with an electronic (phonon) band gap in the range of 0.25 eV to 1.26 eV (12.01 cm^{-1} to 90.71 cm^{-1}). Interestingly, some flat bands appear around the Fermi level for all chlorinated phosphorene with a width in the range of 22 meV to 580 meV. The calculated storage capacity of chlorinated phosphorene is 168.19 mA h g^{-1} and the average open-circuit voltage is estimated to be 2.08 V acceptable for use as a cathode in ClBs. Our findings suggest that phosphorene is a good candidate to be used as cathode material in ClBs.

Acknowledgments N. Hassani acknowledges ISEF support. Part of this work is funded within the framework of the HSE University Basic Research Program. M. Yagmurcukardes was partially supported by the BAGEP Award of the Science Academy with funding supplied by the Sevinc-Erdal Inonu Foundation.

[1] P. Bridgman, Journal of the American chemical society **36**, 1344 (1914).

[2] M. Ghaedi, *Photocatalysis: Fundamental Processes and Applications* (Academic Press, 2021).

[3] F. Wang, Z. Wang, L. Yin, R. Cheng, J. Wang, Y. Wen, T. A. Shifa, F. Wang, Y. Zhang, X. Zhan, *et al.*, Chemical Society Reviews **47**, 6296 (2018).

[4] V. Musle and S. Choudhary, Optical and Quantum Electronics **50**, 1 (2018).

[5] Z. Yi, M. Wu, and R. Jia, Journal of Materials Science **57**, 5482 (2022).

[6] X. Tang, W. Liang, J. Zhao, Z. Li, M. Qiu, T. Fan, C. S. Luo, Y. Zhou, Y. Li, Z. Guo, *et al.*, Small **13**, 1702739 (2017).

[7] T. Liu, Y. Liu, M. Chen, X. Guo, S. Tang, R. Zhang, Z. Xie, J. Wang, A. Gu, S. Lin, *et al.*, Advanced Functional Materials **32**, 2106779 (2022).

[8] Q. Yang, W. Xiong, L. Zhu, G. Gao, and M. Wu, Journal of the American Chemical Society **139**, 11506 (2017).

[9] N. Lu, Z. Zhuo, Y. Wang, H. Guo, W. Fa, X. Wu, and X. C. Zeng, The journal of physical chemistry letters **9**, 6568 (2018).

[10] H. Xu, D. Liu, W. Wang, and G. Yu, Inorganic Chemistry **61**, 3121 (2022).

[11] Z.-L. Xu, S. Lin, N. Onofrio, L. Zhou, F. Shi, W. Lu, K. Kang, Q. Zhang, and S. P. Lau, Nature Communications **9**, 1 (2018).

[12] J. Pang, A. Bachmatiuk, Y. Yin, B. Trzebicka, L. Zhao, L. Fu, R. G. Mendes, T. Gemming, Z. Liu, and M. H. Rummeli, Advanced Energy Materials **8**, 1702093 (2018).

[13] K. Pu, X. Dai, D. Jia, W. Tao, F. Liu, X. Zhang, J. Song, T. Zhao, and Y. Hao, Journal of Alloys and Compounds **812**, 152125 (2020).

[14] M. Park, H. Bae, S. Lee, L. Yang, and H. Lee, Journal of Physics: Condensed Matter **28**, 305301 (2016).

[15] H. Sahin and S. Ciraci, The Journal of Physical Chemistry C **116**, 24075 (2012).

[16] S. J. Clark, M. D. Segall, C. J. Pickard, P. J. Hasnip, M. I. Probert, K. Refson, and M. C. Payne, Zeitschrift für kristallographie-crystalline materials **220**, 567 (2005).

[17] J. P. Perdew, K. Burke, and M. Ernzerhof, Physical Review Letters **77**, 3865 (1996).

[18] S. Grimme, Journal of computational chemistry **27**, 1787 (2006).

[19] B. Delley, The Journal of Chemical Physics **113**, 7756 (2000).

[20] Q. He, B. Yu, Z. Li, and Y. Zhao, Energy & Environmental Materials **2**, 264 (2019).

[21] X. Zhao, S. Ren, M. Bruns, and M. Fichtner, Journal of Power Sources **245**, 706 (2014).

[22] Q. Yin, D. Rao, G. Zhang, Y. Zhao, J. Han, K. Lin, L. Zheng, J. Zhang, J. Zhou, and M. Wei, Advanced Functional Materials **29**, 1900983 (2019).

[23] X. Zhao, Z. Zhao, M. Yang, H. Xia, T. Yu, and X. Shen, ACS Applied Materials & Interfaces **9**, 2535 (2017).

[24] F. Chen, Z. Y. Leong, and H. Y. Yang, Energy Storage Materials **7**, 189 (2017).

[25] X. Zhao, Z. Zhao-Karger, D. Wang, and M. Fichtner, Angewandte Chemie **125**, 13866 (2013).

[26] A. Castellanos-Gomez, The journal of physical chemistry letters **6**, 4280 (2015).

[27] J. Qiao, X. Kong, Z.-X. Hu, F. Yang, and W. Ji, Nature Communications **5**, 1 (2014).

[28] W. Li, Y. Yang, G. Zhang, and Y.-W. Zhang, Nano Letters **15**, 1691 (2015).

[29] A. Khelif, B. Aoubiza, S. Mohammadi, A. Adibi, and V. Laude, Physical Review E **74**, 046610 (2006).

[30] A. Khelif, P. Deymier, B. Djafari-Rouhani, J. O. Vasseur, and L. Dobrzynski, Journal of Applied Physics **94**, 1308 (2003).

[31] Y. Tian, G. Zeng, A. Rutt, T. Shi, H. Kim, J. Wang, J. Koettgen, Y. Sun, B. Ouyang, T. Chen, *et al.*, Chemical Reviews **121**, 1623 (2020).

[32] C. Yang, S. Xin, L. Mai, and Y. You, Advanced Energy Materials **11**, 2000974 (2021).

[33] E. Olsson, J. Yu, H. Zhang, H.-M. Cheng, and Q. Cai, Advanced Energy Materials , 2200662 (2022).

[34] Q. Yin, J. Zhang, J. Luo, J. Han, M. Shao, and M. Wei, Chemical Engineering Journal **389**, 124376 (2020).

[35] Q. Yin, J. Luo, J. Zhang, L. Zheng, G. Cui, J. Han, and D. O'Hare, Journal of Materials Chemistry A **8**, 12548 (2020).

[36] Z. Zhang, X. Hu, Y. Zhou, S. Wang, L. Yao, H. Pan, C.-Y. Su, F. Chen, and X. Hou, Journal of Materials Chemistry A **6**, 8244 (2018).

[37] P. Gao, M. A. Reddy, X. Mu, T. Diemant, L. Zhang, Z. Zhao-Karger, V. S. K. Chakravadhanula, O. Clemens, R. J. Behm, and M. Fichtner, Angewandte Chemie **128**, 4357 (2016).

[38] T. Yu, Q. Li, X. Zhao, H. Xia, L. Ma, J. Wang, Y. S. Meng, and X. Shen, ACS Energy Letters **2**, 2341 (2017).

[39] M. Wu, M. Ma, J. Wang, R. Wang, X. Shi, H. Zhang, C. Jin, Y. Wei, and R. Lian, Energy Storage Materials **51**, 80 (2022).

[40] X. Hu, F. Chen, S. Wang, Q. Ru, B. Chu, C. Wei, Y. Shi, Z. Ye, Y. Chu, X. Hou, *et al.*, ACS Applied Materials & Interfaces **11**, 9144 (2019).

[41] Q. Yin, J. Luo, J. Zhang, S. Zhang, J. Han, Y. Lin, J. Zhou, L. Zheng, and M. Wei, Advanced Functional Materials **30**, 1907448 (2020).

[42] J. Luo, Q. Yin, J. Zhang, S. Zhang, L. Zheng, and J. Han, ACS Applied Energy Materials **3**, 4559 (2020).

[43] Q. Zhang, R. Karthick, X. Zhao, L. Zhang, Y. Shi, L. Sun, C.-Y. Su, and F. Chen, Nanoscale **12**, 12268 (2020).

[44] Z. Zhao, T. Yu, Y. Miao, and X. Zhao, Electrochimica Acta **270**, 30 (2018).

[45] X. Han, C. Liu, J. Sun, A. D. Sendek, and W. Yang, RSC Advances **8**, 7196 (2018).

[46] W.-C. Chang, K.-W. Tseng, and H.-Y. Tuan, Nano Letters **17**, 1240 (2017).

[47] X. Xiao, M. Wang, J. Tu, and S. Jiao, Physical Chemistry Chemical Physics **21**, 7021 (2019).

Supplementary Information: "Chlorinated phosphorene for energy application: electronic and phonon properties "

N. Hassani,[1,*] M. Yagmurcukardes,[2] F. M. Peeters,[3,4] and M. Neek-Amal[1,5,†]

[1] *Department of Physics, Shahid Rajaee Teacher Training University, 16875-163 Lavizan, Tehran, Iran.*

[2] *Department of Photonics, Izmir Institute of Technology, 35430 Izmir, Turkey.*

[3] *Departamento de Física, Universidade Federal do Ceará, 60455-760 Fortaleza, Ceará, Brazil.*

[4] *HSE University, Moscow, 101000 Russia.*

[5] *Departement Fysica, Universiteit Antwerpen, Groenenborgerlaan 171, B-2020 Antwerpen, Belgium.*

* nasim.hassani.chem@gmail.com

† mehdi.neekamal@gmail.com

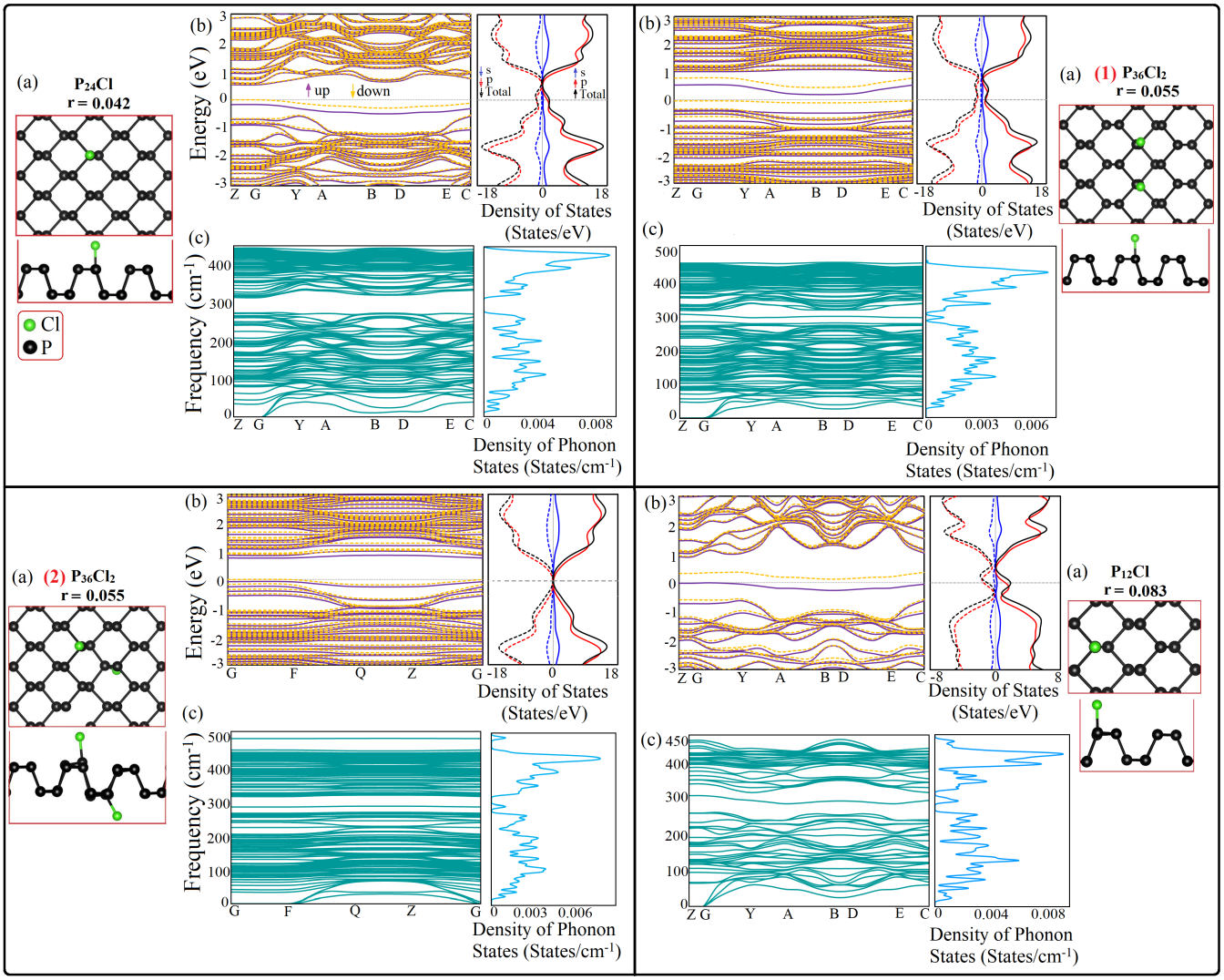

FIG. S1. Top and side views of P_mCl_n ($r = m/n = 0.043, 0.055, 0.083$) with Cl bonded on one or two sides are shown in the corner of each panel. The electronic band structure (Left) and the electronic density of states (Right) are depicted in the top of each panel. The phonon band structure (Left) and the phonon density of states (Right) are demonstrated in the bottom of each panel. The numbers in parentheses refer to the different structures for the same value of r (see Table I).

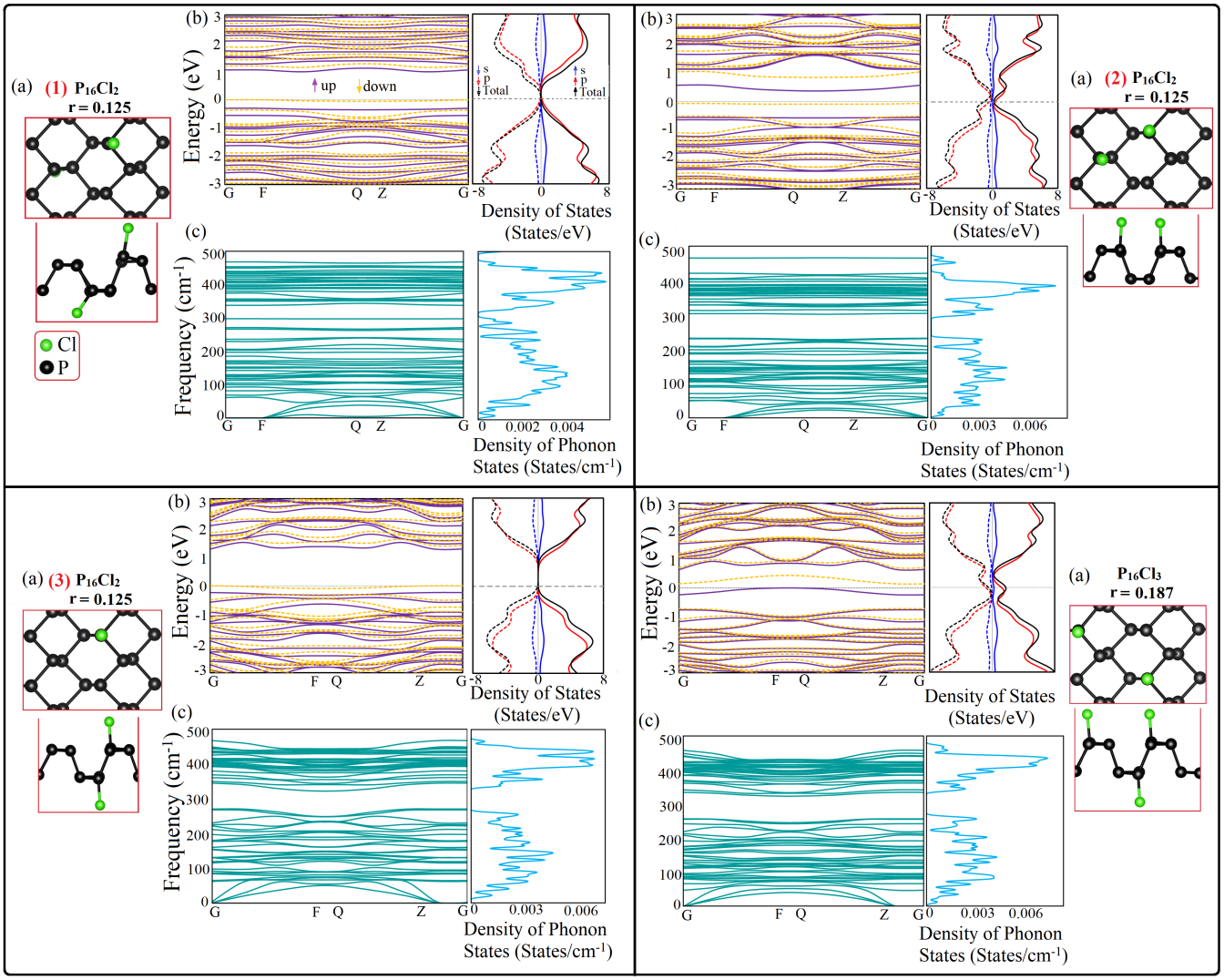

FIG. S2. Top and side views of P_mCl_n ($r = m/n = 0.125, 0.187$) with Cl bonded on one or two sides are shown in the corner of each panel. The electronic band structure (Left) and the electronic density of states (Right) are depicted in the top of each panel. The phonon band structure (Left) and the phonon density of states (Right) are demonstrated in the bottom of each panel. The numbers in parentheses refer to the different structures for the same value of r (see Table I).

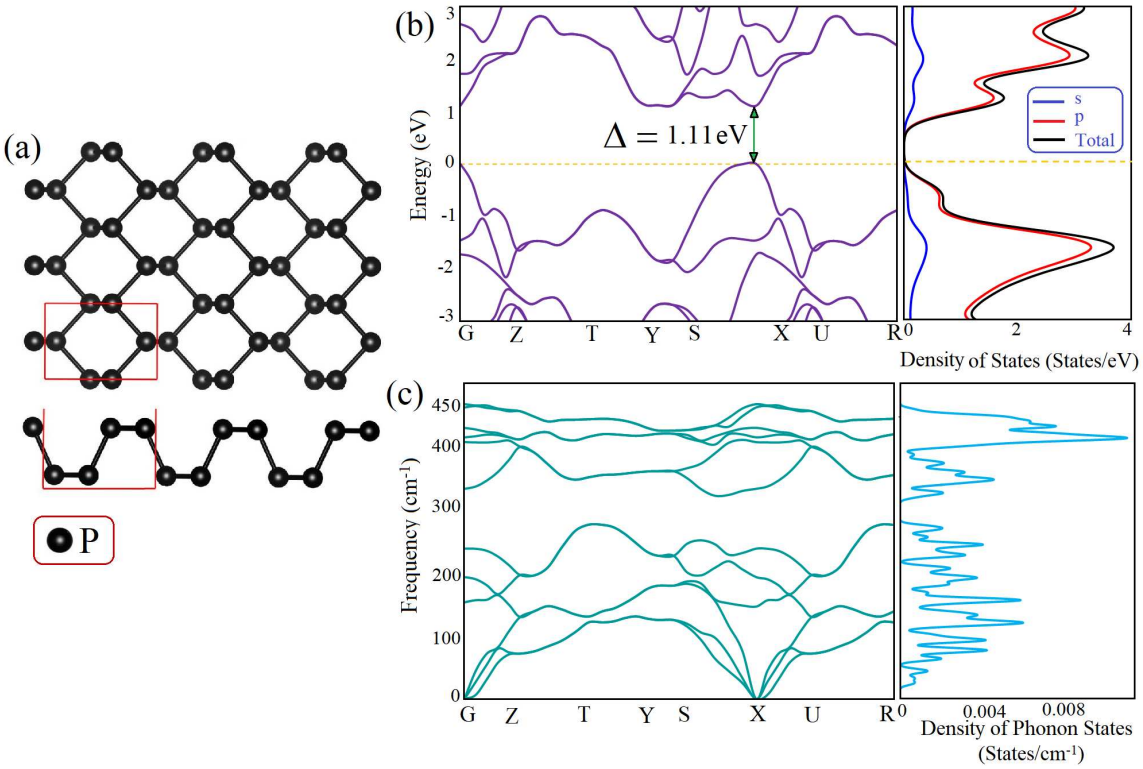

FIG. S3. (a) Left: The electronic band structure; Right: The electronic density of states. (b) Left: The phonon band structure; Right: The phonon density of states of the pristine phosphorene.